

Optical Potential for Light Nuclei and Momentum-Space Eikonal Phase Function

C. M. Werneth^{a,*}, K. Maung Maung^b, M. D. Vera^b, L. W. Townsend^c

^a*NASA Langley Research Center, 2 West Reid Street, Hampton, VA 23681*

^b*University of Southern Mississippi, Department of Physics and Astronomy, 118 College Dr., Box 5046, Hattiesburg, MS 39406*

^c*University of Tennessee, Department of Nuclear Engineering, 315 Pasqua Engineering Building, Knoxville, TN 37996*

Abstract

One way of predicting nuclear cross sections is to use the Eikonal method, a high energy (small scattering angle) approximation that depends on the nucleus-nucleus optical potential. In the position-space representation, the optical potential is a 6-dimensional integral over projectile and target densities and the nucleon-nucleon transition amplitude. The integration is often performed numerically and is inefficient, especially when the task is to compute large numbers of nuclear cross sections for various projectile-target reactions. The aim of the current work is to present two efficient methods for the computation of the Eikonal phase shift function. Analytic formulas of the optical potential are presented in the position-space representation for nuclei that are well-represented by harmonic-well nuclear matter densities ($A < 20$), which reduces the Eikonal phase factor to an integration over a single dimension. Next, the Eikonal phase function is presented in the momentum-space representation, which is particularly useful when the Fourier transform of the position-space optical potential is known. These new methods increase the computational efficiency by three orders of magnitude and allow for rapid prediction of elastic differential, total, elastic, and reaction cross sections in the Eikonal approximation.

Keywords: Eikonal approximation, Elastic differential cross sections

1. Introduction

2 The Eikonal approximation is a high energy (small angle) scattering approximation of
3 the Lippmann-Schwinger (LS) equation that is used for the prediction of total, elastic, re-
4 action, and elastic differential cross sections [1]. It is well-suited for the prediction of cross
5 sections for projectile nuclei with kinetic energies in the laboratory frame greater than
6 approximately 150 MeV/n, as was shown in recent comparisons to the non-relativistic
7 partial wave (PW) decomposition and three-dimensional LS solution methods [2, 3]. All

8 physical observables are computed from the scattering amplitude that is obtained by in-
9 tegrating the Eikonal phase function in the scattering plane. The Eikonal phase function
10 is related to the optical potential and depends on the model of the nuclear interaction.

11 Multiple scattering theory (MST) is the underlying theory upon which the optical
12 potential is derived [4]. In the non-relativistic MST, the unperturbed Hamiltonian can
13 be separated from the residual interaction that is modeled as individual nucleon-nucleon
14 (NN) interactions. Feshbach et al. [5, 6] showed that the transition amplitude, which
15 can be used to obtain the physical observables, may be expressed as an equivalent set of
16 equations known as the elastic scattering equation and the optical potential. With this
17 formalism, the projectile and target remain in the ground state after colliding, and the
18 excited states are included through the optical potential, which is then written such that
19 the leading term is the sum of Watson- τ operators (pseudo two-body operators). The
20 matrix element of the optical potential is found after making several approximations, such
21 as the impulse, single scattering, optimum factorization, and on-shell approximations
22 [2, 3, 7, 8]. The final result is an optical potential that depends on the projectile and
23 target nuclear charge densities and the free NN transition amplitude, which may be
24 parameterized to experimental data.

25 The NN transition amplitude used in the current work satisfies the optical theorem
26 and depends on parameterizations of the total NN cross section, slope parameter, and
27 real-to-imaginary ratio [2, 3]. Electron scattering experiments are used to estimate the
28 charge density of nuclei. Harmonic-well and Woods-Saxon nuclear charge density mod-
29 els are often utilized for the evaluation of the optical potential [9–14]. Harmonic-well
30 densities are used for lighter nuclei ($A < 20$) because of the Gaussian-like decay of the
31 nuclear charge density as a function of radial distance. Woods-Saxon densities are better
32 suited for heavier nuclei, where the nuclear charge density is relatively constant before
33 decreasing to zero at larger radial distances.

34 The fundamental particles participating in the interaction must be specified in any
35 MST. In this study, nuclei are composite particles whose fundamental constituents are
36 nucleons; the quark structure of the nucleons is not considered. It is expected that the
37 inner structure of the nucleons would be probed at higher energies, and these effects
38 are assumed to be included in the NN parameterizations. The nuclear charge density
39 is found by folding the nuclear matter density with the charge density of the proton
40 in the position-space representation [10]. The Fourier transform of the position-space
41 nuclear charge density can then be written as the product of the momentum-space proton
42 charge density and nuclear matter density. The nuclear charge densities were obtained
43 in the momentum-space representation, and the nuclear matter densities were found by
44 dividing the nuclear charge density by the Gaussian charge distribution of the proton.
45 The position-space nuclear matter densities for light nuclei modeled with the harmonic-
46 well density were obtained by computing the Fourier transform of the momentum-space
47 nuclear matter density.

48 In the position-space representation, the optical potential is a 6-dimensional integral
49 over the projectile and target nuclear matter densities and the NN transition amplitude
50 [10, 13–17]. An additional integral is performed over the z -direction of the scattering
51 plane to obtain the Eikonal phase function. In the momentum-space representation,
52 the optical potential is the product of the nuclear matter densities and NN transition
53 amplitude as a function of momentum transfer [3]. The aim of this work is to present two
54 methods for computation of the Eikonal phase function so that the scattering amplitude

55 and nuclear cross sections can be found efficiently.

56 Using the Gaussian forms of the nuclear matter densities and transition amplitude for
57 light nuclei ($A < 20$) in the position-space representation, exact analytic expressions for
58 the optical potential for nucleon-nucleus (NA) and nucleus-nucleus (AA) scattering are
59 presented. This approach effectively reduces the 7-dimensional integral for the Eikonal
60 phase factor in the position-space representation to an integral over 1-dimension. This
61 method is not used for heavier projectile and target nuclei since no closed form solution
62 was found for the optical potential.

63 Another approach is needed for heavier projectile or target nuclei. The Eikonal phase
64 factor is presented in the momentum-space representation, which also reduces the number
65 of integrations to 1-dimension. This method may be used when the optical potential
66 is expressed in momentum-space or when the Fourier transforms of the position-space
67 nuclear matter densities and transition amplitude are known in the momentum-space
68 representation.

69 This paper is organized as follows. In section 2, the optical potential and Eikonal scat-
70 tering theory are reviewed. The nuclear matter densities and NN transition amplitudes–
71 and their corresponding Fourier transforms–are explicitly defined, and the exact formulas
72 for NA and AA optical potentials are given for light nuclei ($A < 20$). Next, the opti-
73 cal potential is expressed as a function of momentum transfer, and the 7-dimensional
74 integral of the Eikonal phase factor is reduced to a 1-dimensional integral when the
75 momentum-space optical potential is used.

76 In section 3, elastic differential cross sections for light nuclei reactions are predicted
77 with the analytic formulas and are compared to elastic differential cross sections produced
78 from the numerically integrated optical potential. It is demonstrated that the light
79 nuclei formulas for the optical potential produce elastic differential cross sections that
80 are in exact agreement with the numerically integrated optical potential. Next, the
81 momentum-space formulation of the Eikonal phase factor is used to compute the elastic
82 differential cross sections and compared to the differential cross sections as computed with
83 the optical potential in the position-space representation. The Eikonal phase function in
84 the momentum-space representation produces results that are in exact agreement with
85 the position-space results. The conclusions are given in section 4.

86 2. Theory

87 The Eikonal scattering amplitude, $f(\theta)$, is needed to compute the elastic differential,
88 reaction, total, and elastic cross sections and is given by [1]

$$f(\theta) = \frac{k}{i} \int_0^{\infty} J_0(2kb \sin(\theta/2)) \left[e^{i\chi(k,b)} - 1 \right] b db, \quad (1)$$

89 where b is the impact parameter, k is the relative momentum of the projectile-target
90 system in the center of mass (CM) frame, $\chi(k, b)$ is the Eikonal phase shift function,
91 $J_0(kb)$ is the cylindrical Bessel function, and θ is the scattering angle in the CM frame.
92 The Eikonal phase function is found by integrating the optical potential, $U(b, z)$, in the
93 z -direction of the scattering plane, which is defined to be in the same direction as that

94 of the incident projectile [1]:

$$\chi(k, b) = -\frac{1}{2k} \int_{-\infty}^{\infty} U(b, z) dz. \quad (2)$$

95 The elastic differential cross section is given by

$$\frac{d\sigma}{d\Omega} = |f(\theta)|^2, \quad (3)$$

and the total elastic cross section is found by integrating over the polar and azimuthal angles [1],

$$\begin{aligned} \sigma_{\text{el}} = \int \frac{d\sigma}{d\Omega} d\Omega &= 4\pi \int_0^{\infty} [1 - e^{-\text{Im}\chi} \cos(\text{Re}\chi)] b db \\ &\quad - 2\pi \int_0^{\infty} [1 - e^{-2\text{Im}\chi}] b db. \end{aligned}$$

96 The scattering amplitude satisfies the optical theorem, therefore [1]

$$\sigma_{\text{tot}} = \frac{4\pi}{k} \text{Im}f(\theta = 0) = 4\pi \int_0^{\infty} [1 - e^{-\text{Im}\chi} \cos(\text{Re}\chi)] b db. \quad (4)$$

97 Finally, the reaction cross section, σ_{re} , can be found from using $\sigma_{\text{re}} = \sigma_{\text{tot}} - \sigma_{\text{el}}$.

98 All of the the cross sections described above are functions of the Eikonal phase func-
99 tion and depend on the optical potential, as shown in equation (2). For AA scattering,
100 the optical potential may be expressed as [10, 15]

$$U(\mathbf{r}) = A_P A_T \int t_{\text{NN}}(|\mathbf{r}_{\text{NN}}|) \rho_P(|\mathbf{r}_P|) \rho_T(|\mathbf{r}_T|) d\mathbf{r}_T d\mathbf{r}_{\text{NN}}, \quad (5)$$

101 where A is the number of nucleons, P represents the projectile, T represents the target,
102 t_{NN} is the NN transition amplitude, and ρ is the nuclear matter density. As illustrated in
103 Fig. 1, \mathbf{r}_{NN} is the vector between a nucleon in the projectile and a nucleon in the target;
104 \mathbf{r}_P is the vector that extends from the center of the projectile nucleus to a nucleon in the
105 projectile; \mathbf{r}_T is the vector between the center of the target nucleus to a nucleon in the
106 target; \mathbf{r} is the relative distance between the centers of the projectile and target nuclei;
107 $\mathbf{R} = \mathbf{r} + \mathbf{r}_T$ is the distance from the center of the projectile to a nucleon in the target.
108 The distance from the center of the projectile nucleus to a nucleon in the projectile may
109 be expressed as $\mathbf{r}_P = \mathbf{r} + \mathbf{R} = \mathbf{r} + \mathbf{r}_T + \mathbf{r}_{\text{NN}}$, which, when substituted into equation (5),
110 leads to

$$U(\mathbf{r}) = A_P A_T \int t_{\text{NN}}(|\mathbf{r}_{\text{NN}}|) \rho_P(|\mathbf{r} + \mathbf{r}_T + \mathbf{r}_{\text{NN}}|) \rho_T(|\mathbf{r}_T|) d\mathbf{r}_T d\mathbf{r}_{\text{NN}}. \quad (6)$$

111 (Note that $|\mathbf{r}| = \sqrt{b^2 + z^2}$ in the cylindrical coordinate system and that the $d\mathbf{r}$ notation
 112 refers to the differential volume element, which is also written as d^3r .) In the next
 113 section, the nuclear matter densities are described.

114 *2.1. Nucleon-nucleon transition amplitude and nuclear matter density*

115 In the current work, elastic differential cross sections are predicted with the Eikonal
 116 approximation utilizing the position-space representation and the momentum-space rep-
 117 resentation of the optical potential, which is a function of the nucleon-nucleon (NN)
 118 transition amplitude and nuclear matter densities. In this section, the position-space
 119 representation and Fourier transforms of the NN transition amplitude and nuclear mat-
 120 ter densities are given.

121 Usually, harmonic-well nuclear matter densities are used for $A < 20$, and Woods-
 122 Saxon matter densities are used for $A \geq 20$ [10, 15]. The harmonic-well nuclear matter
 123 density in position-space is [10]

$$\rho^{\text{HW}}(r) = \frac{\rho_0^{\text{HW}} a^3}{8s^3} \left[\left(1 + \frac{3\gamma}{2} - \frac{3\gamma a^2}{8s^2}\right) + \frac{\gamma a^2}{16s^4} r^2 \right] \exp\left[\frac{-r^2}{4s^2}\right], \quad (7)$$

124 where

$$\rho_0^{\text{HW}} = \frac{1}{\pi^{3/2} a^3 \left[1 + \frac{3}{2}\gamma\right]}, \quad (8)$$

125 γ and a are parameters given in references [11, 12], $s^2 = a^2/4 - r_{\text{prot}}^2/6$, and r_{prot} is
 126 the proton radius [10, 15]. The Fourier transform of the harmonic-well nuclear matter
 127 density is given by [10]

$$\rho^{\text{HW}}(q) = \rho_0^{\text{HW}} \pi^{3/2} a^3 \left[\left(1 + \frac{3}{2}\gamma\right) - \frac{a^2 \gamma}{4} q^2 \right] e^{-q^2 s^2}. \quad (9)$$

128 The Woods-Saxon nuclear charge density is given as [10]

$$\rho^{\text{WS}}(r) = \frac{\rho_0^{\text{WS}}}{1 + e^{\frac{r-R}{c_A}}}, \quad (10)$$

129 where the normalization is

$$\rho_0^{\text{WS}} = \frac{3}{4\pi} \left[\frac{1}{R^3 + \pi^2 c_A^2 R} \right]. \quad (11)$$

130 R is the half density radius, and c_A is a parameter that is related to the surface diffuseness,
 131 c , by [10]

$$c_A = \frac{2r_p}{\sqrt{3}} \ln \left[\left(\frac{3\beta - 1}{3 - \beta} \right) \right]^{-1} \quad (12)$$

132 and

$$\beta = \exp \left[\frac{r_{\text{prot}}}{c\sqrt{3}} \right], \quad (13)$$

133 where r_{prot} is the proton radius. The parameters R and c are given in references [11, 12].

134 The Fourier transform of the Woods-Saxon charge density is [7]

$$\rho^{\text{WS}}(q) = \frac{4\pi}{q} \rho_0^{\text{WS}} \phi(q), \quad (14)$$

where

$$\begin{aligned} \phi(q) = \pi c_A R \left[\frac{-\cos(qR)}{\sinh(qc_A\pi)} + \frac{\pi c_A}{R} \frac{\sin(qR) \coth(qc_A\pi)}{\sinh(qc_A\pi)} \right. \\ \left. - \frac{2c_A}{\pi R} \sum_{n=1}^{\infty} \frac{(-1)^n n q c_A}{[(qc_A)^2 + n^2]^2} \right]. \end{aligned} \quad (15)$$

135 The NN transition amplitude is given by [10].

$$t_{\text{NN}}(r) = -\sqrt{\frac{e}{m_{\text{prot}}}} \frac{1}{[2\pi B(e)]^{(3/2)}} \sigma(e) [\kappa(e) + i] e^{-r^2/2B(e)}, \quad (16)$$

136 where e is the kinetic energy of the NN system in the CM frame, m_{prot} is the proton
137 mass, $B(e)$ is the slope parameter, $\sigma(e)$ is the NN cross section, and $\kappa(e)$ is the real to
138 imaginary ratio of the NN cross section.

139 The Fourier transform of the NN transition amplitude is given as [10]

$$t_{\text{NN}}(q) = \frac{-1}{(2\pi)^2} \frac{\hbar^2}{\mu} \frac{k\sigma(e)}{4\pi} [\kappa(e) + i] e^{B(e)q^2/2} \quad (17)$$

140 where \hbar is Planck's constant, μ is the reduced mass of the NN system, and k is the
141 relative momentum in the NN CM frame.

142 2.2. Analytical Expressions of the Optical Potential

143 In this section, the analytic expressions for the optical potential are presented for
144 nuclei with $A < 20$, where harmonic-well nuclear matter densities have been used. To
145 simplify the notation, the harmonic-well nuclear matter densities are written

$$\rho(r) = (\alpha + \beta r^2) \exp\left[\frac{-r^2}{4s^2}\right], \quad (18)$$

146 where

$$\alpha = \frac{\rho_0^{\text{HW}} a^3}{8s^3} \left[1 + \frac{3\gamma}{2} - \frac{3\gamma a^2}{8s^2} \right] \quad (19)$$

147 and

$$\beta = \frac{\rho_0^{\text{HW}} a^3}{8s^3} \frac{\gamma a^2}{16s^4}, \quad (20)$$

148 and the NN transition amplitude is written as

$$t(r) = \tau \exp\left[\frac{-r^2}{2B(e)}\right], \quad (21)$$

149 with

$$\tau = -\sqrt{\frac{e}{m_p}} \frac{\sigma(e)}{[2\pi B(e)]^{3/2}} [\kappa(e) + i]. \quad (22)$$

150 Two cases are considered. First, the optical potential is calculated for a single nucleon
 151 projectile and a target nucleus. Next, the calculation is repeated for a projectile nucleus
 152 and a target nucleus.

153 *2.2.1. Nucleon-Nucleus Optical Potential*

154 For nucleon-nucleus (NA) collisions, the single projectile nucleon matter density is
 155 taken as a Dirac delta function, and the harmonic-well nuclear matter density from
 156 equation (18) is used for the target. The optical potential from equation (6) may be
 157 expressed in the following form with $A_P = 1$:

$$U(r) = (C_0 + C_1 r^2) \exp[-C_2 r^2] \quad (23)$$

158 with

$$C_0 = \tau A_T \left(\frac{\pi}{\mu_1 + \mu_2} \right)^{3/2} \left[\alpha_T + \frac{3\beta_T}{2(\mu_1 + \mu_2)} \right], \quad (24)$$

159

$$C_1 = \frac{\tau \beta_T A_T \mu_1^2 \pi^{3/2}}{(\mu_1 + \mu_2)^{7/2}}, \quad (25)$$

160 and

$$C_2 = \mu_1 - \frac{\mu_1^2}{(\mu_1 + \mu_2)}, \quad (26)$$

161 where

$$\mu_1 = \frac{1}{2B} \quad \text{and} \quad \mu_2 = \frac{1}{4s_T^2}. \quad (27)$$

162 It should be noted that C_0 and C_1 are complex, because both are functions of τ from
 163 equation (22).

164 *2.2.2. Nucleus-Nucleus Optical Potential*

165 The calculation of the optical potential is repeated for nucleus-nucleus (AA) collisions
 166 with harmonic-well nuclear matter densities for both the projectile and the target, which
 167 results in the following formula for the optical potential:

$$U(r) = (A_0 + A_1 r^2 + A_2 r^4) \exp[-A_3 r^2], \quad (28)$$

168 where

$$\begin{aligned} A_0 &= \frac{2\pi N A_P A_T}{\theta} \sqrt{\frac{\pi}{\theta}} \\ &\times \left[\frac{\alpha_T \Lambda_1}{2} + \frac{3}{4\theta} (\beta_T \Lambda_1 + \Lambda_2 \alpha_T) \right. \\ &\quad \left. + \frac{15\Lambda_2 \beta_T}{8\theta^2} \right], \end{aligned} \quad (29)$$

$$\begin{aligned}
A_1 &= \frac{2\pi N A_P A_T}{\theta} \sqrt{\frac{\pi}{\theta}} \\
&\times \left[\frac{\alpha_T \Lambda_2}{2} + \frac{1}{4\theta} (3\Lambda_2 \beta_T - 4\alpha_T \Lambda_2 \delta) \right. \\
&+ \frac{\delta}{2\theta^2} (\beta_T \Lambda_1 \delta + \Lambda_2 \alpha_T \delta - 5\beta_T \Lambda_2) \\
&\left. + \frac{5\delta^2 \Lambda_2 \beta_T}{2\theta^3} \right], \tag{30}
\end{aligned}$$

$$\begin{aligned}
A_2 &= \frac{2\pi N A_P A_T}{\theta} \sqrt{\frac{\pi}{\theta}} \\
&\times \left[\frac{\Lambda_2 \beta_T \delta^2}{2\theta^2} - \frac{\beta_T \Lambda_2 \delta^3}{\theta^3} + \frac{\Lambda_2 \beta_T \delta^4}{2\theta^4} \right], \tag{31}
\end{aligned}$$

169 and

$$A_3 = \delta - \frac{\delta^2}{\theta} \tag{32}$$

170 where

$$N = \frac{2\pi\tau}{\kappa} \sqrt{\frac{\pi}{\kappa}}, \tag{33}$$

$$\kappa = \frac{1}{4s_P^2} + \frac{1}{2B} \tag{34}$$

$$\theta = \frac{1}{4s_T^2} + \delta, \tag{35}$$

$$\delta = \frac{1}{4s_P^2} - \frac{1}{16s_P^4 \kappa}, \tag{36}$$

$$\Lambda_1 = \frac{\alpha_P}{2} + \frac{3\beta_P}{4\kappa}, \tag{37}$$

171 and

$$\Lambda_2 = \frac{\beta_P}{2} + \frac{\beta_P}{32\kappa^2 s_P^4} - \frac{\beta_P}{4\kappa s_P^2}. \tag{38}$$

172 Ultimately, A_0 , A_1 , and A_2 are complex since each depends on N from equation (33).

173 The authors would like to acknowledge that Bidasaria and Townsend [18, 19] have
174 studied this problem independently, but the results were not published. In the next sec-
175 tion, the optical potential is written as a function of momentum transfer, which leads to
176 more efficient evaluation of cross sections when exact expressions for the optical potential
177 are not known.

178 *2.3. Optical Potential in Momentum-Space*

179 In section 2, it was shown that the Eikonal phase function can be obtained by
 180 integrating the optical potential in the position-space representation. In this section, the
 181 optical potential is expressed as a function of momentum transfer, \mathbf{q} . By doing so, the
 182 number of integration dimensions will be significantly reduced.

To begin, the NN transition amplitude and nuclear matter densities in equation (6)
 are replaced with their Fourier transforms

$$U(\mathbf{r}) = \frac{A_P A_T}{(2\pi)^6} \int d\mathbf{r}_T d\mathbf{r}_{NN} d\mathbf{q}_1 d\mathbf{q}_2 d\mathbf{q}_3 [t_{NN}(|\mathbf{q}_1|)\rho_T(|\mathbf{q}_2|)\rho_P(|\mathbf{q}_3|) \quad (39)$$

$$\times e^{-i\mathbf{q}_1 \cdot \mathbf{r}_{NN}} e^{-i\mathbf{q}_2 \cdot \mathbf{r}_T} e^{-i\mathbf{q}_3 \cdot (\mathbf{r} + \mathbf{r}_T + \mathbf{r}_{NN})}],$$

183 where the Fourier transforms are given by

$$t_{NN}(\mathbf{r}) = \int t_{NN}(\mathbf{q}) e^{-i\mathbf{q} \cdot \mathbf{r}} d\mathbf{q} \quad (40)$$

184 and

$$\rho(\mathbf{r}) = \frac{1}{(2\pi)^3} \int p(\mathbf{q}) e^{-i\mathbf{q} \cdot \mathbf{r}} d\mathbf{q}. \quad (41)$$

185 Note that because of the traditional normalization of nuclear matter densities, the nor-
 186 malizations for the Fourier transforms of $\rho(\mathbf{r})$ and $t_{NN}(\mathbf{r})$ differ. Next, integration over
 187 \mathbf{r}_T and \mathbf{r}_{NN} is performed by using the the delta distribution,

$$\delta(\mathbf{A}) = \frac{1}{(2\pi)^3} \int e^{-i\mathbf{A} \cdot \mathbf{B}} d\mathbf{B}, \quad (42)$$

188 which results in

$$U(\mathbf{r}) = A_P A_T \int t(|\mathbf{q}_1|)\rho_T(|\mathbf{q}_2|)\rho_P(|\mathbf{q}_3|)\delta(\mathbf{q}_1 + \mathbf{q}_3)\delta(\mathbf{q}_1 + \mathbf{q}_2)e^{-i\mathbf{q}_3 \cdot \mathbf{r}} d\mathbf{q}_1 d\mathbf{q}_2 d\mathbf{q}_3. \quad (43)$$

189 After evaluating the delta functions, the optical potential from equation (39) is reduced
 190 to integration over the momentum transfer,

$$U(\mathbf{r}) = \int U(\mathbf{q}) e^{i\mathbf{q} \cdot \mathbf{r}} d\mathbf{q}, \quad (44)$$

191 where $U(\mathbf{q}) = A_P A_T t_{NN}(|\mathbf{q}|)\rho_P(|\mathbf{q}|)\rho_T(|\mathbf{q}|)$.

Next, the Fourier transform of the optical potential (44) is substituted into the ex-
 pression for the Eikonal phase shift function from equation (2),

$$\chi(k, b) = -\frac{1}{2k} \int_{-\infty}^{\infty} dz \int U(\mathbf{q}) e^{i\mathbf{q} \cdot (\mathbf{z} + \mathbf{b})} d\mathbf{q} \quad (45)$$

$$= -\frac{1}{2k} \int_{-\infty}^{\infty} dz d\mathbf{q} U(\mathbf{q}) e^{i\mathbf{q} \cdot \mathbf{b}} e^{iqz \cos \theta},$$

192 where $\mathbf{r} = \mathbf{b} + \mathbf{z}$ in cylindrical coordinates has been used. The integration of z is
 193 performed, which results in

$$\chi(k, b) = -\frac{\pi}{k} \int \frac{1}{q} \delta(\cos \theta) U(\mathbf{q}) e^{i\mathbf{q}\cdot\mathbf{b}} d\mathbf{q}, \quad (46)$$

194 where the following delta distribution has been used:

$$\frac{2\pi}{q} \delta(\cos \theta) = \int_{-\infty}^{\infty} e^{iqz \cos \theta} dz. \quad (47)$$

Using $d\mathbf{q} = q^2 dq \sin \theta d\theta d\phi$ and evaluating the delta distribution leads to the final form for the Eikonal phase function,

$$\chi(k, b) = -\frac{\pi}{k} \int_0^{\infty} dq \int_0^{2\pi} q U(|\mathbf{q}|) e^{iqb \cos \phi} d\phi \quad (48)$$

$$= \frac{-2\pi^2}{k} \int_0^{\infty} q U(q) J_0(qb) dq. \quad (49)$$

195 The advantage of equation (49) is that the 6-dimensional integral for the optical po-
 196 tential in position-space, and the z integration need not be performed. Instead, the
 197 7-dimensional integral for χ has been reduced to 1-dimension over the magnitude of the
 198 momentum transfer, q . This result significantly increases the efficiency for the numerical
 199 evaluation of χ .

200 3. Results

201 The optical potential depends on parameterizations of the nuclear matter density
 202 and NN transition amplitude. The harmonic-well nuclear matter density parameters for
 203 ^{16}O used in equations (18) - (20) are $\gamma = 1.544$ and $\alpha = 1.83$ fm [11, 12]. The NN
 204 transition amplitude depends on parameterizations of the NN total cross section, the
 205 real to imaginary ratio of the transition amplitude, and the slope parameter. Parame-
 206 terizations of the proton-proton and neutron-proton cross sections are from reference [3].
 207 The proton-proton and neutron-proton real to imaginary ratio of the transition ampli-
 208 tude was obtained by fitting to data in reference [20], and the NN slope parameter is
 209 from reference [10]. In the current work, the isospin average of the proton-proton and
 210 neutron-proton parameterizations were used for both the total NN cross section and the
 211 real to imaginary ratio of the transition amplitude. The transition amplitude parameters
 212 for total projectile kinetic energies in the laboratory frame of 497 MeV and 1120 MeV
 213 are given in Table 1.

214 The formulas for the optical potential from section 2.2 are used to predict the differen-
 215 tial cross sections for $p + ^{16}\text{O}$ and $^{16}\text{O} + ^{16}\text{O}$ reactions at total projectile kinetic energies
 216 in the laboratory frame of 497.5 MeV and 1120 MeV, respectively. The results of the
 217 new formulas are compared to the numerically integrated results and experimental data

218 [21, 22] in Figs. 2 and 3. The solid black circles with error bars indicate experimental
 219 data [21, 22]. The solid red lines show the result of using the analytically integrated
 220 optical potential, and the blue stars result from using the numerically integrated optical
 221 potential. The analytical results are verified numerically.

222 Fig. 2 shows the elastic differential cross section of a $p + {}^{16}\text{O}$ reaction with a total
 223 projectile kinetic energy in the laboratory frame of 497 MeV. The figure shows that the
 224 differential cross section predicted with the new formula for proton-nucleus collisions
 225 agrees with the cross section that was generated by numerically integrating the optical
 226 potential. Furthermore, both results are in good agreement with experimental data given
 227 in reference [21]. The elastic differential cross section of a ${}^{16}\text{O} + {}^{16}\text{O}$ reaction at a total
 228 projectile kinetic energy in the laboratory frame of 1120 MeV is shown in Fig. 3. Note
 229 that the cross section predicted with the AA formula for the optical potential agrees
 230 exactly with numerical calculation, and each are in good agreement with experimental
 231 data from reference [22].

232 As examples of the momentum-space formulation of the Eikonal phase function, the
 233 elastic differential cross section of $p + {}^{16}\text{O}$ and $\alpha + {}^{20}\text{Ne}$ reactions are computed with
 234 equation (2) in the position-space representation (the usual way of performing the calcu-
 235 lation) and equation (49), which is a function of momentum transfer in the new formula-
 236 tion. These results are shown in Figs. 4 and 5. The position-space Eikonal calculations
 237 are shown with a solid red line, and the momentum-space results are given with blue
 238 stars. Experimental data [23, 24] are presented as black circles with error bars.

239 The harmonic-well nuclear matter density parameters needed for equations (18) and
 240 (9) are $\gamma = 0$ and $a = 1.33$ fm for α -particles, and $\gamma = 1.88$ and $a = 1.54$ fm for ${}^{16}\text{O}$
 241 [11, 12]. The Woods-Saxon nuclear matter density parameters used in equations (10),
 242 (13), and (14) for ${}^{20}\text{Ne}$ are $R = 1.88$ fm and $c = 0.57$ fm. The values of the NN transition
 243 amplitude are given in Table 1 for total projectile kinetic energies in the laboratory frame
 244 of 104 MeV and 317 MeV.

245 The elastic differential cross section for a $p + {}^{16}\text{O}$ reaction at a total projectile kinetic
 246 energy in the laboratory frame of 317 MeV is given in Fig. 4. Experimental data for
 247 this reaction are from reference [23]. Note that the position-space and momentum-space
 248 calculations are in good agreement with experimental data. Also note that the position-
 249 space and momentum-space results are in agreement. Fig. 5 shows the elastic differential
 250 cross section for $\alpha + {}^{20}\text{Ne}$ at a total projectile kinetic energy in the laboratory frame
 251 of 104 MeV. The experimental data are from reference [24]. Again, note that both the
 252 position and momentum-space results are in agreement, and each are in good agreement
 253 with experimental data. The predictions of the differential cross sections are less accurate
 254 at larger angles. This is expected behavior, since the Eikonal method is a high energy
 255 and small angle approximation.

256 Although comparisons to experimental data have been shown, it should be stressed
 257 that agreement with experimental data is not the objective of this work. The objective
 258 was to present the two approaches of computing the Eikonal phase function to allow
 259 for efficient computation of nuclear cross sections. The computational time required for
 260 convergence of the position-space optical potential is approximately 10^3 seconds. The
 261 new methods described herein require only a few seconds of computational time thus
 262 providing a three orders of magnitude increase in computational efficiency.

263 **4. Conclusions**

264 The AA optical potential may be used with Eikonal scattering theory to predict elastic
265 differential, total, total elastic, and total reaction cross sections. The optical potential
266 is obtained by computing a 6-dimensional integral over the nuclear matter densities of
267 the projectile and target and the NN transition amplitude. Consequently, numerical
268 evaluation of the optical potential is inefficient.

269 In the current work, NA and AA optical potential formulas were obtained with
270 harmonic-well nuclear matter densities, which are suitable for light nuclei ($A < 20$).
271 The formulas were used to predict the elastic differential cross sections for two light nu-
272 clei reactions. The results generated from the exact optical potentials were verified with
273 numerical integration, and it was found that the elastic differential cross sections are in
274 good agreement with experimental data. The new methods presented herein are approx-
275 imately 1000 times more efficient than the position-space representation calculations.

276 The authors have also shown that the Eikonal phase function can be written as a
277 1-dimensional integral by expressing the optical potential as a function of momentum
278 transfer, thereby greatly increasing the efficiency of the numerical evaluation of cross
279 sections using the Eikonal approximation. The momentum-space formulation of the
280 Eikonal phase function is used to evaluate the differential cross section of two reactions
281 which utilize different nuclear matter density parameterizations. It is found that the
282 momentum-space phase function agrees exactly with the Eikonal approximation com-
283 puted in position-space, and the results of both calculations are in good agreement with
284 experimental data.

285 It has been demonstrated that the optical potential can be evaluated analytically for
286 light ions ($A < 20$) that are modeled with harmonic-well nuclear matter densities. The
287 momentum-space formulation is better suited for nuclear collisions where the projectile
288 or target has mass $A \geq 20$. The Eikonal phase function can be evaluated numerically for
289 *any* transition amplitude and nuclear matter density, provided their Fourier transforms
290 can be computed. Still, analytical expressions of the optical potential should be used
291 when available. Based on the work presented herein, it is recommended that the exact
292 expressions should be used for light ions, and the momentum-space optical potential
293 should be used for all other reactions.

294 **Acknowledgments**

295 This work was supported, in part, by NASA grants NNX13AH31A (University of
296 Southern Mississippi) and NNX16AG01A (University of Tennessee).

297 **References**

- 298 [1] C. J. Joachain, Quantum Collision Theory, American Elsevier, New York, NY, 1983.
299 [2] C. M. Werneth, K. M. Maung, W. P. Ford, J. W. Norbury, M. D. Vera, Elastic differential cross
300 sections for space radiation applications, Phys. Rev. C 90 (2014) 064905.
301 [3] C. M. Werneth, K. M. Maung, W. P. Ford, J. W. Norbury, M. D. Vera, Elastic Differential Cross
302 Sections, NASA/TP-2014-218529.
303 [4] K. M. Watson, Multiple scattering and the many-body problem—applications of photomeson pro-
304 duction in complex nuclei, Phys. Rev. 89 (1953) 575.
305 [5] H. Feshbach, Unified theory of nuclear reactions, Ann. Phys. 5 (1958) 357.

- 306 [6] H. Feshbach, A unified theory of nuclear reactions II, *Ann. Phys.* 19 (1962) 287.
- 307 [7] D. H. Wolfe, Studies of the nucleon-nucleus first order optical potential, Ph.D. thesis, Kent State
- 308 University (1983).
- 309 [8] A. Picklesimer, P. C. Tandy, R. Thaler, D. Wolfe, Momentum space approach to microscopic effects
- 310 in elastic proton scattering, *Phys. Rev. C* 30 (1984) 1861.
- 311 [9] C. M. Werneth, K. M. Maung, L. R. Mead, S. R. Blattnig, Finite sum expressions for elastic and
- 312 reaction cross sections, *Nucl. Instr. Methods in Phys. Res. B* 308 (2013) 40.
- 313 [10] J. W. Wilson, et al., Transport methods and interactions for space radiations, NASA/RP-1991-1257.
- 314 [11] C. W. De Jager, H. De Vries, C. De Vries, Nuclear charge- and magnetization-density-distribution
- 315 parameters from elastic electron scattering, *Atom. Data Nucl. Data* 14 (1974) 479.
- 316 [12] H. De Vries, C. W. De Jager, C. De Vries, Nuclear charge-density-distribution parameters from
- 317 elastic electron scattering, *Atom. Data Nucl. Data* 36 (1987) 495.
- 318 [13] L. W. Townsend, J. W. Wilson, H. B. Bidasaria, On the geometric nature of high energy nucleus-
- 319 nucleus reaction cross sections, *Can. J. Phys.* 60 (1982) 1514.
- 320 [14] L. W. Townsend, Abrasion cross sections for ^{20}Ne projectiles at 2.1 GeV/nucleon, *Can. J. Phys.* 61
- 321 (1983) 93.
- 322 [15] L. W. Townsend, H. B. Bidasaria, J. W. Wilson, Eikonal phase shift analyses of carbon-carbon
- 323 scattering, *Can. J. Phys.* 61 (1983) 867.
- 324 [16] J. W. Wilson, Multiple scattering of heavy ions, Glauber theory, and optical model, *Phys. Lett. B*
- 325 52 (1974) 419.
- 326 [17] J. W. Wilson, L. W. Townsend, An optical model for composite nuclear scattering, *Can. J. Phys.*
- 327 59 (1981) 1569.
- 328 [18] H. B. Bidasaria, L. W. Townsend, Analytic optical potentials for nucleon-nucleus and nucleus-
- 329 nucleus collisions involving light and medium nuclei, NASA/TM-1982-83224.
- 330 [19] L. W. Townsend, H. B. Bidasaria, Analytic determinations of single-folding optical potentials,
- 331 NASA/TM-1983-84611.
- 332 [20] J. W. Wilson, C. M. Costner, Nucleon and heavy-ion total and absorption cross section for selected
- 333 nuclei, NASA/TN-1975-D-8107.
- 334 [21] B. S. Flanders, et al., Empirical density-dependent effective interaction for nucleon-nucleus scatter-
- 335 ing at 500 MeV, *Phys. Rev. C* 43 (1991) 2103.
- 336 [22] D. T. Khoa, W. von Oertzen, H. G. Bohlen, F. Nuoffer, Study of diffractive and refractive structure
- 337 in the elastic $^{16}\text{O}+^{16}\text{O}$ scattering at incident energies ranging from 124 to 1120 MeV, *Nucl. Phys.*
- 338 A 672 (2000) 387.
- 339 [23] J. J. Kelly, et al., Effective interaction for $^{16}\text{O}(\text{p,p})$ at $\epsilon_p=318$ MeV, *Phys. Rev. C* 43 (1991) 1272.
- 340 [24] H. Rebel, G. W. Schweimer, G. Schatz, J. Specht, R. Lohken, G. Hauser, D. Habs, H. Klewe-
- 341 Nebenius, Quadrupole and hexadecapole deformation of 2s-1d shell nuclei, *Nucl. Phys. A* 182 (1972)
- 342 145.

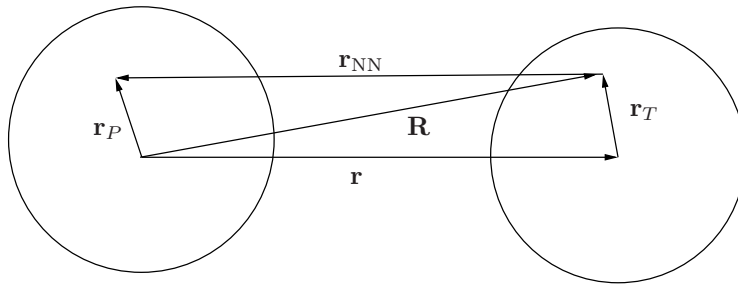


Figure 1: Illustration of the vectors used for the AA optical potential. The distance from the center of the projectile nucleus to a nucleon in the projectile nucleus is \mathbf{r}_P . Likewise, \mathbf{r}_T is the distance from the center of the target nucleus to a nucleon in the target. The center to center distance between nuclei is \mathbf{r} , and \mathbf{r}_{NN} is the distance between a nucleon in the projectile to a nucleon in the target. $\mathbf{R} = \mathbf{r} + \mathbf{r}_T$ is the distance from the center of the projectile to a nucleon in the target.

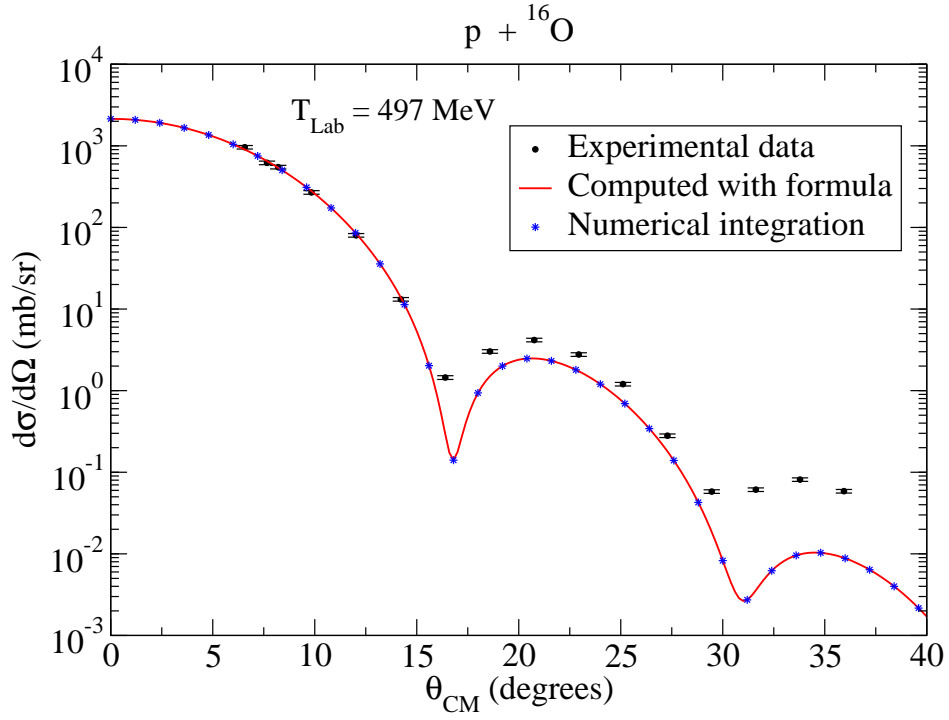


Figure 2: The elastic differential cross section for a $p + {}^{16}\text{O}$ reaction with a total projectile kinetic energy in the laboratory frame of 497 MeV. Experimental data are from reference [21].

Table 1: Energy dependent parameters for the NN transition amplitude.

Lab Energy	σ (fm ²)	B (fm ²)	κ
104 MeV	21.80	0.22	0.88
317 MeV	3.02	0.32	0.41
497 MeV	3.52	0.34	0.18
1120 MeV	7.16	0.26	0.96

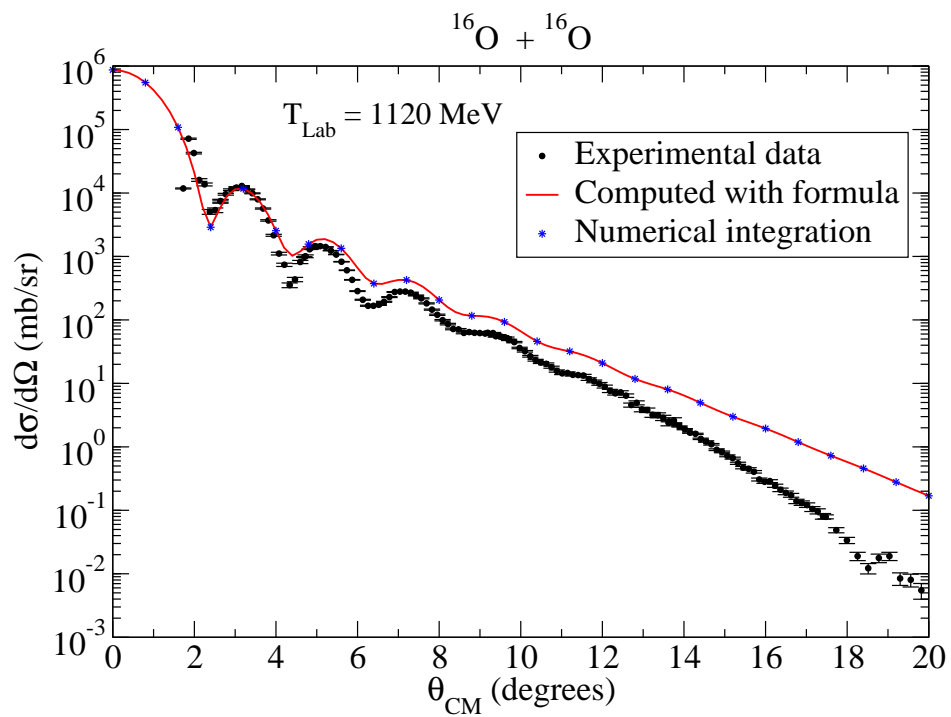


Figure 3: The elastic differential cross section of the $^{16}\text{O} + ^{16}\text{O}$ reaction with a total projectile kinetic energy in the laboratory frame of 1120 MeV. Experimental data are from reference [22].

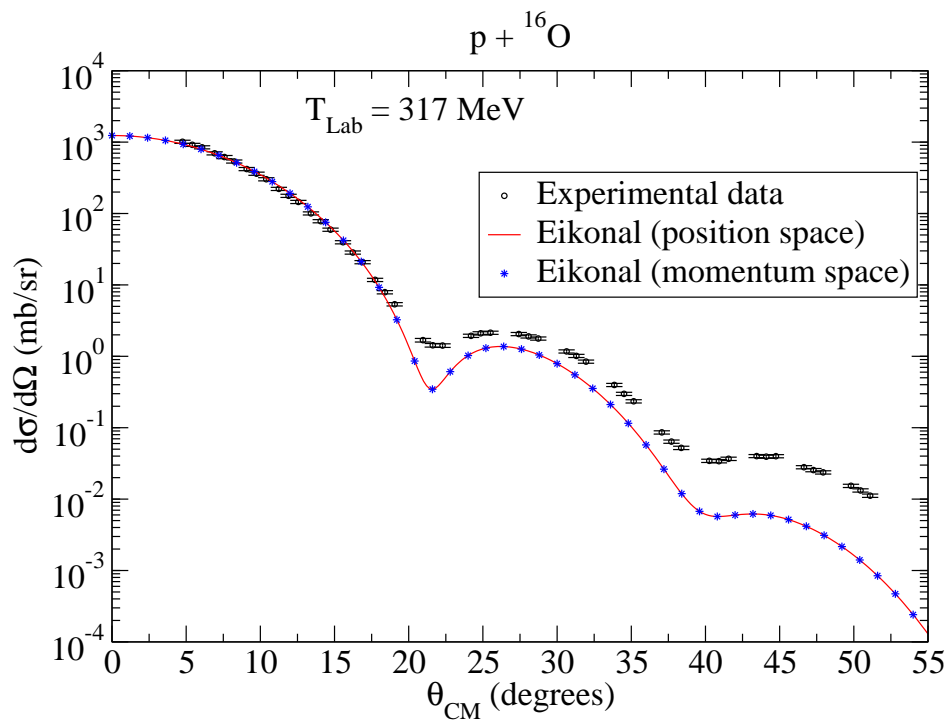


Figure 4: The elastic differential cross section for a $p + {}^{16}\text{O}$ reaction at a total projectile kinetic energy in the laboratory frame of 317 MeV. Experimental data are from reference [23].

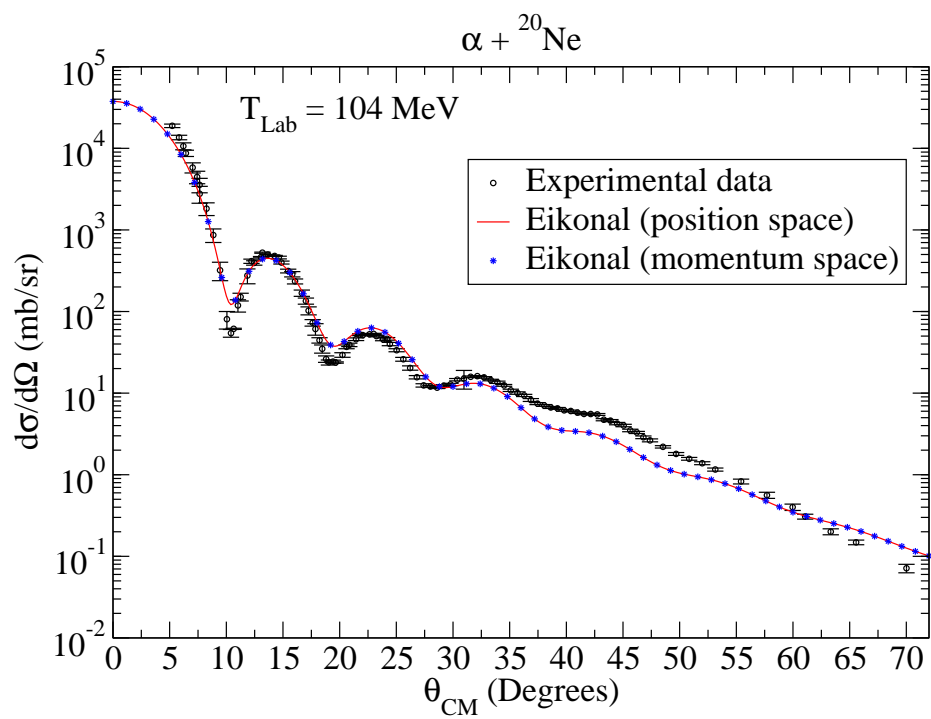


Figure 5: The elastic differential cross section for a $\alpha + {}^{20}\text{Ne}$ reaction at a total projectile kinetic energy in the laboratory frame of 104 MeV. Experimental data are from reference [24].